Coulomb-Driven Energy Boost of Heavy Ions for Laser-Plasma Acceleration

J. Braenzel,[1,2,*] A. A. Andreev,[1,3,4] K. Platonov,[3] M. Klingsporn,[5] L. Ehrentraut,[1] W. Sandner,[1,2,6] and M. Schnürer[1]
[1]*Max Born Institute, Max Born Strasse 2A, 12489 Berlin, Germany*
[2]*Technical University Berlin, Strasse des 17. Juni 135, 10623 Berlin, Germany*
[3]*Vavilov State Optical Institute, Birzhevaya line 12, 199064 St. Petersburg, Russia*
[4]*St. Petersburg University, University emb.7, St. Petersburg 199034, Russia*
[5]*IHP, Im Technologiepark 25, 15236 Frankfurt, Germany*
[6]*ELI-DC International Association AISBL, Platanenallee 6, Zeuthen 15738, Germany*
(Received 7 September 2014; published 26 March 2015)

An unprecedented increase of kinetic energy of laser accelerated heavy ions is demonstrated. Ultrathin gold foils have been irradiated by an ultrashort laser pulse at a peak intensity of 8×10^{19} W/ cm^2. Highly charged gold ions with kinetic energies up to >200 MeV and a bandwidth limited energy distribution have been reached by using 1.3 J laser energy on target. 1D and 2D particle in cell simulations show how a spatial dependence on the ion's ionization leads to an enhancement of the accelerating electrical field. Our theoretical model considers a spatial distribution of the ionization inside the thin target, leading to a field enhancement for the heavy ions by Coulomb explosion. It is capable of explaining the energy boost of highly charged ions, enabling a higher efficiency for the laser-driven heavy ion acceleration.

DOI: 10.1103/PhysRevLett.114.124801 PACS numbers: 41.75.Jv, 52.38.-r, 52.59.Dk

Laser driven ion acceleration has gained wide scientific interest, as it is a promising ion source for investigation in basic plasma physics and for application in accelerator technology [1,2] related to biomedical [3,4] and hadron research [5]. While the acceleration of protons and light ions have been intensively investigated during the last decade, little has been reported on acceleration of heavier ions [6]. Such knowledge is mandatory to achieve the objectives of upcoming new laser facilities [7,8], e.g., the exploration of nuclear and astrophysical questions as well as the potential use as beam lines for heavy ion radiotherapy [9]. Energies of heavy ions exceeding the mass number $A \gg 12$ with $E_{\mathrm{kin}}/\mathrm{u} \sim 1$–$2$ MeV/u (energy per nucleon) have been reported so far [6,10], by using short-pulse laser systems with laser pulse energies well above 20 J [11].

In the following, we report and discuss a considerable energy boost for acceleration of highly charged heavy ions by only using 1.3 J on an ultrathin heavy material target. We accelerated ions up to $E_{\mathrm{max}}/u > 1$ MeV/u, with a bandwidth limited energy distribution. We found a remarkable deviation in the maximum energy to charge Z scaling in comparison to established models of Mora [12] and Schreiber [13,14].

Presently used laser ion acceleration schemes like target normal sheath acceleration [15], or leaky light sail and radiation pressure acceleration [16–18], coherent acceleration of ions by laser [4,19], or break out afterburner [20] make use of an energy transfer from laser to electrons and in a following step from electrons to ions. In the typical physical picture, an ultraintense laser pulse is focused on a thin target, ionizes it, and displaces the electrons from the ion background. This creates a high electrical field at the rear and front side of the target. The Coulomb attraction field of the ions circumvents the electrons' escape and enables the acceleration of the ions. For ultrathin targets and relativistic laser intensities, the acceleration is enhanced by the transparency of the target and the relativistic kinematics of the electrons [18,21–23]. Further optimization for the energies of light ions is proposed by a Coulomb exploding background of heavy ion constituents in an ultrathin foil target [24–26]. A remarkable contribution by the Coulomb explosion to the energy of very heavy ion energy is predicted but still under theoretical discussion [27,28].

Most acceleration models assume an averaged degree of ionization leading to a fixed electron density—which creates the moving accelerating electrical field for the ions. During the laser-plasma interaction, ions of different charge-to-mass ratio Z/A separate in the velocity picture, leading to higher MeV/u for the lighter material. The energy per nucleon decreases significantly with the decreasing charge-to-mass ratio, as the accelerating field is screened by the light ions. Laser-plasma experiments using thin foils showed that, in the presence of hydrogen and carbon, ions with a smaller Z/A ratio are not accelerated at all or stay with much lower velocity [10]. Only specially prepared, heated targets without contamination by light ions, enabled an acceleration of the heavy ions up to the MeV/u range. We obtained heavy ions with >1 MeV/u in presence of the contamination layer. While the maximum kinetic energy $E_{\mathrm{kin}}^{\mathrm{max}}$ for hydrogen reaches 12 MeV/u and 4.2 MeV/u for C^{6+}/O^{8+}, the highest charged gold ion $\gtrsim Au^{50+}$ follows with $\gtrsim$1 MeV/u. Experiments have been performed at the Max Born

Institute High Field Ti:sapphire laser. It delivers 1.3 J at (30–35) fs on the target after contrast enhancement by a cross polarized wave generation [29] front end and a double plasma mirror [30], leading to a prepulse free peak-to-amplified spontaneous emission contrast of $\leq 10^{-14}$ in the minor ps range. The laser is focused by an $f/2.5$ of-axis parabola to a focal FHWM size of $\sim 4\ \mu$m, giving an peak intensity of 8×10^{19} W/cm^2. The normalized laser field is $a_0 = qE_L/m_e c\omega = 6$ for linear polarization, with the electron mass m_e and charge q, laser frequency ω, and speed of light c. We focused the laser at freestanding (14 ± 2) nm gold foil [31], which we produced by thermal evaporation at 10^{-6} mbar (deposition rate, 0.2 nm/s), followed by a floating process. High resolution transmission electron microscopy reveals a polycrystalline structure of the gold formed by an island growth mode on a carbon-based supportive film, which we identify as the rest of the parting agent. The average grain size is of the order of 10 nm. Determination of the composition has been carried out by energy dispersive x-ray spectroscopy with a state-of-the-art FEI ChemiSTEM system and was quantified standardless with a Cliff-Lorimer calculation. The foil consists of gold 96%, carbon 2%–3%, and oxygen 2%; hydrogen is not determined. Scanning transmission electron microscopy measurements reveal a sub-crack-like structure in (10–20) nm distance [see Fig. 3(b)]. Structured surfaces can increase the absorption of the laser light, leading to a higher efficiency of the acceleration mechanism. This is at the moment discussed widely, but has not yet been considered for the thinnest targets [32,33]. Accelerated particles were detected in single shot measurement by a Thomson spectrometer at 0° in the laser propagation direction. The setup consists of an entering pinhole with a diameter of 110 μm, a permanent magnet, electrical field plates and a multichannel plate detector, covering a detection angle of 1×10^{-7} sr from the target [34]. Measurements at a lower laser contrast (without double plasma mirror) $\leqq 10^{-11}$, showed much lower $E_{\mathrm{kin}}^{\mathrm{max}}$ and particle numbers for hydrogen, carbon, oxygen ions and no gold ion spectra in the measured energy range.

Figure 1 shows a captured picture of the detector. We identify traces of accelerated gold particles for ionization degrees reaching from Au^{1+} to $> Au^{50+}$, well beyond the C^{3+} trace. With increasing charge-to-mass ratio, we observe light ion traces of oxygen, carbon, and hydrogen. For a quick interpretation of the measured data, the overlay in Fig. 1 shows lines of constant energy for $m = 197$ u to mark constant energy positions for different charge states on the detector. We observed a strong signal for gold ions between Au^{20+} and the highest degree of ionization $>Au^{50+}$ with kinetic energies from 10 to 200 MeV. The traces exhibit a distinct maximum in particle numbers and a bandwidth limited energy distribution for charge states $Z > 25$. The low energetic cutoff for ions charged $Z < 25$ probably lies beyond the detection range.

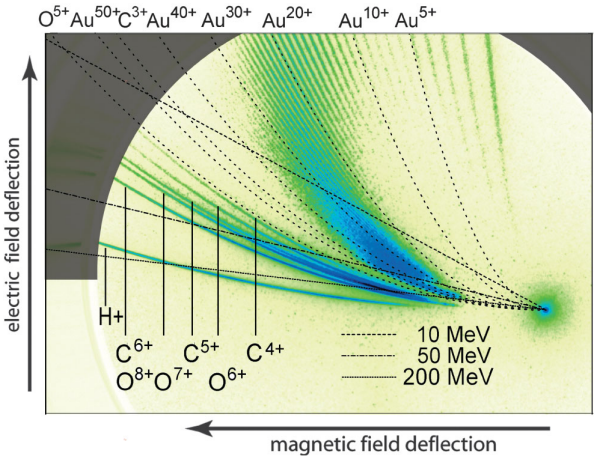

FIG. 1 (color). Raw spectra from Thomson spectrometer (single shot measurement), particle density in false color coding. Each trace represents a different charge-to-mass ratio Z/m. Gray shade indicates end of detector. Light ion traces (H^+, C^{6+}–C^{3+}, O^{8+}–O^{5+}) are identified. Overlay shows theoretical parabolas at different charge states of gold ions (black dots). Straight lines mark theoretical constant energy at each degree of ionization for gold, $m = 197$ u.

The symmetry of the gold ion cutoff on the detector seems to follow a lemniscatelike function (half figure eight): $r[\phi(Z)] \sim a^2 \times 2\sin[2\phi(Z)]$, with a as a constant of the radius and $\phi(Z)$ a nonlinear, charge-depending function. We evaluated the highest energy cutoff and lowest energy cutoff for the different charge states of gold ions in Fig. 2. Compared to an expected $E_{\mathrm{kin}}^{\mathrm{max}} \propto Z^2$ scaling by the model of Ref. [13], our data show a boosted scaling of $E_{\mathrm{kin}}^{\mathrm{max}} \propto (Z-6)^{2.7}$. For a better comparison, Fig. 2 uses the same scaling coefficient for both fit functions. Experiments with gold-coated plastic foils [Formvar (10–40) nm + (2–6) nm gold coating on target rear side] showed similar results concerning the multiple degrees of ionization, the Z to $E_{\mathrm{kin}}^{\mathrm{max}}$ scaling, reaching close to the

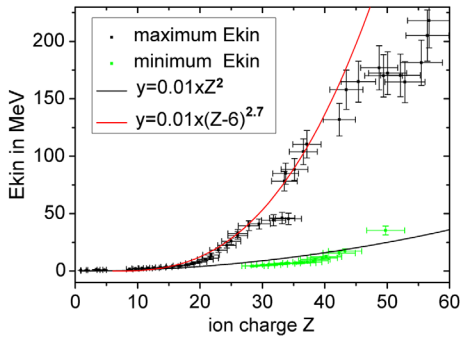

FIG. 2 (color online). Maximum (black) and minimum (green) kinetic energy of gold ions in dependence of their charge state Z. For $Z < 25$, the detector's range is cutting the low energetic part of the spectra. Red line shows a $(Z-6)^{2.7}$ and black line a Z^2 to $E_{\mathrm{kin}}^{\mathrm{max}}$, both fit functions with the same scaling coefficient.

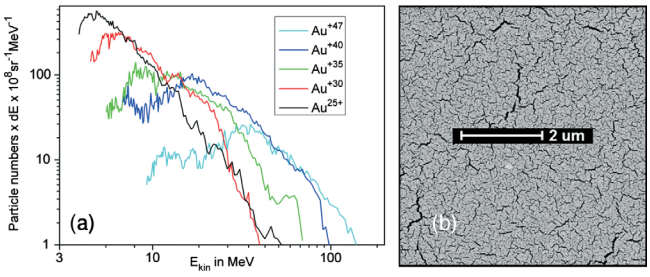

FIG. 3 (color online). (a) The associated evaluated energy distribution for selected, single traces of gold ions of Figs. 1 and 2 is shown, exhibiting a pronounced maximum. dE is given by the binning of the spectrometer's resolution. (b) STEM measurement of freestanding target foil reveals a cracklike structure. Dark cracks mark here the carbon substrate layer.

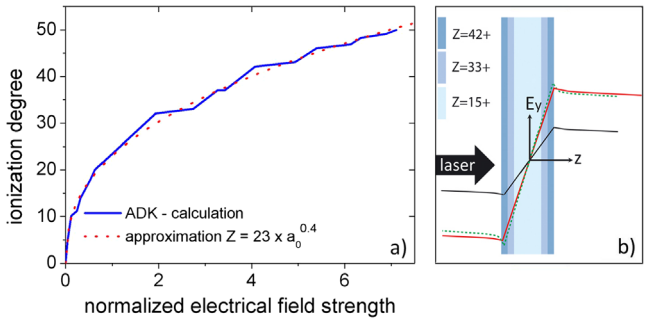

FIG. 4 (color online). (a) The dependence of gold ionization on the electric field E_L in units of a_0 calculated with the Ammasov-Delone-Krainov model. The dashed line (red) fits $Z(a_0) = 23 \times a_0^{0.4}$. (b) E_L calculated from the analytical model (red line) and PIC simulation (green dotted line) considering ion layers of the following degrees of ionization: the distribution of ion charge is 0–1 nm $Z = 42$, 1–2 nm $Z = 33$, 2–18 nm $Z = 15$, 18–19 nm $Z = 33$, 19–20 nm $Z = 42$. Black line, E_L calculated with an averaged ionization degree of $Z = 15$.

MeV/u range, and with a limited bandwidth in the energy spectrum (see the Supplemental Material [35]). This shows a general mechanism for the heavy ion acceleration if the targets thickness is thin enough. The energy distribution related to Fig. 1 of selected gold ions is shown in Fig. 3. The particle numbers are given relative to a detector calibration with hydrogen and carbon, assuming a similar response for heavy ions [36]. The divergence of the heavy ion beam is assumed with 3°, as it is smaller compared to the proton divergence [37]. Here we inferred theoretically from a divergence measurement of the protons (for methods, see the Supplemental Material [35] and Ref. [38]) by using the same acceleration field. Our latest theoretical findings indicate a dependency on charge and mass number [35]. We approximate the energy content of all accelerated gold ions with 5% of the laser energy, while the H^+ reaches <2%.

In order to account for the theoretical ionization Z in dependence on the electrical field strength a_0, we used the Ammasov-Delone-Krainov model [39] as collision ionization is not significant for our case. The calculation for gold is shown in Fig. 3(a) and we find an ionization dependence $Z(a_0) = 23 \times a_0^{0.4}$. The field strength for our parameters considers an intensity of $a_0 = 5$, which leads to a maximum ionization of $Z(a_0) = 42$. Higher ionization as observed in our experiment can be attributed to field enhancement in the case of partly transparent target plasma, to contributions from the surface structure, and to self-focusing.

Our 1D particle in cell (PIC) simulation considered a dynamic ionization and was evaluated at high accuracy (mesh size 0.16 nm, 200 particles per cell, error <1%) and has been performed using the laser parameters of the experiment and a target thickness of 20 nm. For simplification, we froze the ionization in time at the end of the laser pulse. The 1D PIC simulation shows in the longitudinal direction a symmetrical, varying ionization degree $Z(z)$ [see Fig. 4(b)] [40]. Compared to an averaged degree of ionization, it leads to an enhancement of the electrical field at the front and rear side of the target by contributions of the repelling Coulomb force. The field enhancement becomes strong for highly charged ions. For the 2D PIC simulation, we used the ionization distribution of the 1D PIC simulation, at 5×10^{19} W/cm^2, 35 fs, 4 μm focus diameter, Gaussian laser profile. The pulse interacts with a pure 20-nm-thick gold target. The step size of the calculation was 0.5 nm with 30 particles per cell. In Fig. 5, we compare the calculated energies with our experimental results and the model of Ref. [13]. The $E_{\mathrm{kin}}^{\mathrm{max}}$ to Z dependence has to be separated into three parts: while for $Z < 15$, the Au ion energies fit to a $E_{\mathrm{kin}}^{\mathrm{max}} \sim Z^2$, ions with $Z > 15$ are with an exponent >2, followed by a smaller linear dependence for $Z > 42$.

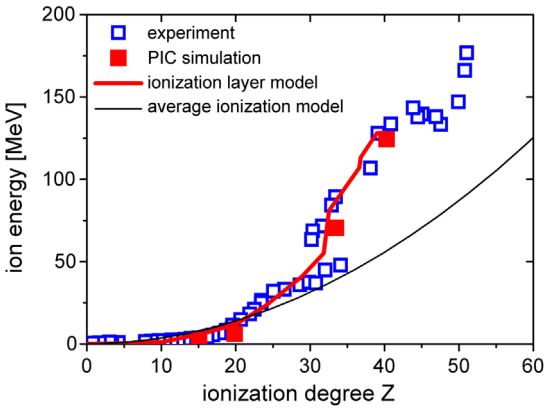

FIG. 5 (color online). The dependence of maximal ion energy on its ionization degree: the experimental data of Fig. 2 are deep blue squares, 2D PIC-simulation data are red squares, the Schreiber model is the black line, and our model is the red line. The distribution of ion ionization is according to the 1D PIC simulation in Fig. 4.

Our analytical model focuses on the Poisson equation, as the electrical field of the laser does not penetrate deep inside even our thin foil. We take a spatially varying ionization of heavy target material into account,

$$2\left(\frac{\partial^2\eta_e}{\partial\xi^2}+\frac{\partial^2\eta_e}{\partial\varsigma^2}\right)=\eta_e-Z(E)\eta_{i0}\Theta\left(\frac{l_f}{2}-|\xi|\right)\Theta\left(\frac{l_e}{2}-|\varsigma|\right). \tag{1}$$

Here, we use a 2D geometry with the coordinates $(z,y)=(\xi,\varsigma)r_D$, where the Debye radius is $r_D^2=T_H/4\pi e^2 n_{eH}$ and assuming the process to be adiabatic. The normalized electron density is $\eta_e=n_e/n_{eH}$ and the normalized electric field is $E=(2c/\omega r_D)(\partial\eta_e/\partial\xi)$. The ion density $n_i(z,y)=\eta_{i0}\Theta(z)\Theta(y)n_{eH}$ has a rectangular shape in both directions, where $L_{f,e}(t)=l_{f,e}(t)r_D$ are dynamic foil thickness and electron spot size, respectively. The hot electron density is determined from quasineutrality and the ionization degree is $Z(E)=23E^{0.4}$. We introduce a spatial dependence of the hot electron density, $n_{eH}\approx(\pi e^2 n_i^2/T_H)[\int_0^{l_{f0}}Z(\xi)d\xi]^2$. The spatial-depending degree of ionization is given as

$$Z(\xi)=23\times\left(\frac{2c}{\omega r_D}\frac{\partial\eta_e}{\partial\xi}\right)^{0.4}. \tag{2}$$

The electron temperature T_H depends on the pulse duration τ_L and on a laser absorption coefficient κ (here and in the following, see Ref. [41]): $T_H(l_f)\approx[\kappa(L_{f0})I_L\tau_L]/n_{eh}L_{f0}$. For simplification, we assume a rectangular transversal (y) and longitudinal (z) electron density profile, which width changes in time with $l_f(t)$. In the case of an ultrathin foil we can rewrite: $\Theta(l_f(t)/2-|\xi|)\to l_f(t)\delta(\xi)$, we take the expansion of the recirculating hot electrons as a time dependent parameter $l_e(t)$. At this point, we freeze the degree of ionization in time. The time-dependent solution of Eq. (1) at $|z|\geq L_f(t)/2$ looks similar to Ref. [41],

$$E(z,y,t)=4\pi e n_{i0}\frac{\mathrm{sgn}(z)\Theta(l_e(t)-|\varsigma|)}{1+\sigma_c \mathrm{tr}_D L_f(t)/D_0^2}\times\int_0^{l_{f0}}Z(\xi)d\xi\exp\left(-|\xi|+\frac{l_{f0}}{2}\right). \tag{3}$$

D_0 denotes the initial electron spot size and σ_c is the plasma conductivity. The equation contains a spatial dependence of the charge distribution in the target instead of an averaged, constant one. The dependence of the analytical field in Eq. (3) on coordinate z is similar to the PIC-simulated one [Fig. 4(b)]. The charged ion front $l_f(t)$ in the target can be calculated by the equation of motion after inserting Eq. (3) and with $C=16\pi e^2 l_{f0}n_{i0}/m_i$,

$$l_f(t)=l_{f0}+t\sqrt{C\times Z(l_{f0})\left[\int_0^{l_{f0}}Z(\xi)d\xi\right]\ln\left[\frac{l_f(t)}{l_{f0}}\right]}. \tag{4}$$

Equation (4) defines the energy of an ion with maximum degree of ionization, which is at the front of acceleration $\varepsilon_{Z(l_{f0})}\approx m_i\dot{L}_f^2(t)/8$. Electron density in each instant is defined by Eq. (1). From the equation of continuity follows $n_i(z,t)=n_i l_{f0}\Theta(l_f/2-|z|)/l_f(t)$ and the ion velocity with the coordinate of z reads $v_i(z,t)=z\dot{l}_f(t)/l_f(t)$, $|z|<l_f(t)/2$. The energy for a particle placed initially at ξ_0 with an charge of $Z(\xi_0)$ has to be evaluated parametrically with Eqs. (2) and (4). For ions inside the target, $\xi_0\epsilon[0,l_f/2]$ results,

$$\varepsilon_z(\xi,t^*)=\frac{m_i}{2}(\xi_0/l_{f0})^2\dot{L}_f^2(t^*). \tag{5}$$

With $t^*\approx D_0^2/\sigma_c r_D l_f$ for ions of very high energy, $t^*\sim 2\tau_L$ [12]. This leads to $\sim Z^3$ ion energy to charge scaling, which is in good agreement with our PIC-simulated and experimental results (see Fig. 5). Ions with a very high degree of ionization $Z>Z(l_{f0})$, are formed in a field maximum at the target rear side. These ions have the initial coordinate $\xi_0=l_{f0}$. According to Eq. (4), $\dot{l}_f\approx Z(l_{f0})$ for ions with a high charge Z, the formula (5) gives for all $Z>42$ the linear relation $\varepsilon_Z\sim Z$. The smaller energy-to-Z scaling is explained by the decreasing charged background compared to ions placed inside the target.

In conclusion, we have demonstrated efficient acceleration of heavy ions by an ultrashort laser pulse system. So far laser systems that compensate lower laser energy with a shorter pulse duration to reach the same intensity had not been able to accelerate heavy ions with $A>12$ into the MeV/u region. By using an ultrathin foil of heavy material, we achieved highly charged heavy ions with a limited bandwidth in the energy spectrum reaching up to 1 MeV/u. Furthermore, we simplified a complex target preparation, which achieves a prerequisite for future applications. We demonstrated experimentally and theoretically how a spatial distribution of the ionization inside the target leads to a field enhancement for the heavy ions by Coulomb explosion. This has the potential to greatly improve the efficiency of heavy ion acceleration by stronger kinetic energy with charge scaling. Our results indicate that, e.g., energies with 7 MeV/u can be achieved with ~50 times higher laser energy than in our experiment. This relaxes the previously estimated laser power requirements for upcoming facilities [7] by a factor of 3 which is enormous in costs if ultrafast ~100 J class lasers are considered.

The research leading to these results received funding from the Deutsche Forschungsgemeinschaft within the

program CRC/Transregio 18 and LASERLAB-EUROPE (Grant No. 284464, EC's Seventh Framework Program). Computational resources were provided by the JSC within Project No. HBU15 and by the John von Neumann Institute for Computing (NIC) providing us access on JUROPA at Jülich Supercomputing Centre. Furthermore we thank D. Sommer for his excellent work on the target production.

*Corresponding author.
braenzel@mbi-berlin.de

[1] T. E. Cowan *et al.*, Phys. Rev. Lett. **92**, 204801 (2004).
[2] V. Scuderi *et al.*, Nucl. Instrum. Methods Phys. Res., Sect. A **740**, 87 (2014).
[3] D. Schardt, T. Elsässer, and D. Schulz-Ertner, Rev. Mod. Phys. **82**, 383 (2010).
[4] T. Tajima, D. Habs, and X. Q. Yan, Rev. Acc. Science Technol. **2**, 201 (2009).
[5] C. Hill, CERN Linac 2, http://linac2.web.cern.ch/linac2/.
[6] M. Hegelich *et al.*, Phys. Rev. Lett. **89**, 085002 (2002).
[7] G. Morou, G. Korn, W. Sandner, and J. L. Collier, *The Whitebook of ELI Nuclear Physics Group* (Thoss-Media GmbH, Berlin, 2011).
[8] H. Daido, M. Nishiuchi, and A. Pirozhkov, Rep. Prog. Phys. **75**, 056401 (2012).
[9] G. Kraft, *Tumor Therapy with Heavy Ions* (Verein zur Förderung der Tumortherapie mit Schweren Ionen e.V., Darmstadt, 2007).
[10] B. M. Hegelich, B. J. Albright, J. Cobble, K. Flippo, S. Letzring, M. Paffett, H. Ruhl, J. Schreiber, R. K. Schulze, and J. C. Fernandez, Nature (London) **439**, 441 (2006).
[11] B. M. Hegelich *et al.*, Phys. Plasmas **12**, 056314 (2005).
[12] P. Mora, Phys. Rev. E **72**, 056401 (2005).
[13] J. Schreiber *et al.*, Phys. Rev. Lett. **97**, 045005 (2006).
[14] J. Schreiber, http://edoc.ub.uni-muenchen.de/5842/1/Schreiber_Joerg.pdf.
[15] S. C. Wilks, A. B. Langdon, T. E. Cowan, M. Roth, M. Singh, S. Hatchett, M. H. Key, D. Pennington, A. MacKinnon, and R. A. Snavely, Phys. Plasmas **8**, 542 (2001).
[16] T. Esirkepov, M. Yamagiwa, and T. Tajima, Phys. Rev. Lett. **96**, 105001 (2006).
[17] B. Qiao, M. Zepf, M. Borghesi, B. Dromey, M. Geissler, A. Karmakar, and P. Gibbon, Phys. Rev. Lett. **105**, 155002 (2010).
[18] A. Henig *et al.*, Phys. Rev. Lett. **103**, 245003 (2009).
[19] X. Q. Yan, C. Lin, Z. M. Sheng, Z. Y. Guo, B. C. Liu, Y. R. Lu, J. X. Fang, and J. E. Chen, Phys. Rev. Lett. **100**, 135003 (2008).
[20] D. Jung *et al.*, Phys. Plasmas **20**, 083103 (2013).
[21] X. Q. Yan, T. Tajima, M. Hegelich, L. Yin, and D. Habs, Appl. Phys. B **98**, 711 (2010).
[22] S. Steinke *et al.*, Laser Part. Beams **28**, 215 (2010).
[23] S. Steinke *et al.*, Phys. Rev. ST Accel. Beams **16**, 011303 (2013).
[24] T. Z. Esirkepov *et al.*, Phys. Rev. Lett. **89**, 175003 (2002).
[25] B. Qiao, S. Kar, M. Geissler, P. Gibbon, M. Zepf, and M. Borghesi, Phys. Rev. Lett. **108**, 115002 (2012).
[26] S. S. Bulanov *et al.*, Phys. Rev. E **78**, 026412 (2008).
[27] H. Y. Wang *et al.*, Phys. Rev. E **89**, 013107 (2014).
[28] A. V. Korzhimanov, E. S. Efimenko, S. V. Golubev, and A. V. Kim, Phys. Rev. Lett. **109**, 245008 (2012).
[29] M. Kalashnikov, K. Osvay, R. Volkov, H. Schönnagel, and W. Sandner, *CLEO-2011—Laser Applications to Photonic Applications* (American Institute of Physics, Melville, New York, 2011), p. CWG3.
[30] A. Levy *et al.*, Opt. Lett. **32**, 310 (2007).
[31] J. Braenzel, C. Pratsch, P. Hilz, C. Kreuzer, M. Schnürer, H. Stiel, and W. Sandner, Rev. Sci. Instrum. **84**, 056109 (2013).
[32] A. A. Andreev and K. Y. Platonov, Contrib. Plasma Phys. **53**, 173 (2013).
[33] T. Ceccotti *et al.*, Phys. Rev. Lett. **111**, 185001 (2013).
[34] T. Sokollik, *Investigations of Field Dynamics in Laser Plasmas with Proton Imaging*, Springer Theses (Springer, Berlin, 2011).
[35] See the Supplemental Material at http://link.aps.org/supplemental/10.1103/PhysRevLett.114.124801 for heavy ion spectra with a different target composition, additional information to account for of the heavy ions divergence and laser to particle energy efficiency.
[36] R. Prasad *et al.*, Nucl. Instrum. Methods Phys. Res., Sect. A **623**, 712 (2010).
[37] E. Brambrink, J. Schreiber, T. Schlegel, P. Audebert, J. Cobble, J. Fuchs, M. Hegelich, and M. Roth, Phys. Rev. Lett. **96**, 154801 (2006).
[38] F. Nürnberg *et al.*, Rev. Sci. Instrum. **80**, 033301 (2009).
[39] M. Ammosov, A. Delone, and V. Krainov, Sov. Phys. JETP **64**, 1191 (1986).
[40] A. Zhidkov and A. Sasaki, Phys. Plasmas **7**, 1341 (2000).
[41] A. A. Andreev, S. Steinke, M. Schnuerer, A. Henig, P. V. Nickles, K. Y. Platonov, T. Sokollik, and W. Sandner, Phys. Plasmas **17**, 123111 (2010).